SLC10A3 promotes liver cancer progression via modulation of the TGF-β signaling pathway

OULI LONG, CHUNLING YANG, MENGMENG YU and PAILAN PENG

Department of Gastroenterology, The Affiliated Hospital of Guizhou Medical University, Guiyang, Guizhou 550009, P.R. China

Received March 12, 2026; Accepted October 26, 2026

DOI: 10.3892/ol.2026.15951

Abstract. While solute carrier family 10 member 3 (SLC10A3) is an oncogene in numerous malignancies, its involvement in liver cancer (LC) progression is not yet well understood. In the present study, western blot (WB) analysis demonstrated elevated SLC10A3 expression in LC cell lines compared with normal liver cell lines. Small interfering RNA was used to knockdown SLC10A3 expression in these cell lines, and transcriptome sequencing was performed on the suppression and control groups to determine the differentially expressed genes (DEGs) and main signaling pathways affected by SLC10A3. Kyoto Encyclopedia of Genes and Genomes analysis illustrated significant enrichment of these DEGs in the transforming growth factor-β (TGF-β) pathway in LC cell lines ($P<0.05$). WB analysis illustrated that SLC10A3 knockdown suppressed TGF-β pathway signaling, reversing epithelial-mesenchymal transition in LC cells. The biological effects of SLC10A3 knockdown were evaluated using colony formation, 5-ethynyl-2'-deoxyuridine, Cell Counting Kit-8, wound healing and Transwell invasion assays. The findings indicated that reducing SLC10A3 expression markedly hindered LC cell aggressiveness ($P<0.05$). Rescue assays were ultimately performed to confirm the observed regulatory mechanisms. The present study found that SLC10A3 was upregulated in LC cells, and its knockdown suppressed cell migration and invasion, which is associated with the TGF-β pathway, illustrating its potential as a target for LC treatment.

Correspondence to: Dr Pailan Peng, Department of Gastroenterology, The Affiliated Hospital of Guizhou Medical University, 28 Guiyi Street, Yunyan, Guiyang, Guizhou 550009, P.R. China
E-mail: pengpailan@163.com

Abbreviations: CCK-8, Cell Counting Kit-8; DEGs, differentially expressed genes; E-cadherin, epithelial cadherin; EdU, 5-ethynyl-2'-deoxyuridine; EMT, epithelial-mesenchymal transition; FBS, fetal bovine serum; FC, fold change; GO, Gene Ontology; KEGG, Kyoto Encyclopedia of Genes and Genomes; LC, liver cancer; PBS, phosphate-buffered saline; p-Smad2, phosphorylated Smad2; p-Smad3, phosphorylated Smad3; siNC, negative control small interfering RNA; SLC10A3, solute carrier family 10 member 3; siSLC10A3, small interfering RNA targeting the SLC10A3 gene; TGF-βR, TGF-β receptor I; TME, tumor microenvironment

Key words: SLC10A3, TGF-β signaling pathway, EMT, LC

Introduction

Liver cancer (LC) is a highly lethal malignancy globally. According to the latest GLOBOCAN 2024 estimates, there were ~843,000 newly diagnosed liver cancer cases and 732,000 cancer-related deaths worldwide in 2024, ranking seventh in cancer incidence but third in cancer mortality across all tumor types (1). Hepatocellular carcinoma is responsible for ~90% of primary LC cases (2). Despite advances in surgical resection, radiotherapy and chemotherapy, LC maintains a high mortality rate due to challenges such as low early diagnosis rates, aggressive invasion and metastasis as well as high postoperative recurrence, yielding a 5-year survival rate of <20% (3,4). The progression of LC is associated with dysregulated signaling pathways, tumor suppressor gene inactivation and oncogene activation (5). Identifying key oncogenes and understanding their molecular mechanisms is important for developing new diagnostic biomarkers and targeted therapies for this disease.

Solute carrier family 10 member 3 (SLC10A3), a key member of the solute carrier superfamily, has been recently recognized as a central oncogene in multiple cancer types. He *et al* (6) illustrated that increased SLC10A3 expression is notably associated with poor survival outcomes and immune infiltration in patients with low-grade glioma. Additionally, Wang *et al* (7) illustrated that SLC10A3 expression is higher in colorectal cancer and is closely associated with poor prognosis. Multispectral imaging combined with bioinformatics analysis indicates that genes of the SLC10 family exhibit close clinical and immune associations with LC, suggesting that SLC10A3 exerts a regulatory effect on immune responses during immunotherapy in LC (8). However, the biological activities and potential molecular mechanisms of SLC10A3 in LC remain to be systematically investigated. Therefore, the present study aimed to examine the function of SLC10A3 in the incidence and progression of LC, as well as its possible regulatory mechanisms, through *in vitro* experiments.

The transforming growth factor-β (TGF-β) pathway has a dual function in regulating tumor initiation and progression. During initial tumor development, TGF-β is considered an anticancer agent that halts cell cycle progression and triggers apoptosis. During tumor progression, TGF-β/Smad signaling

can become aberrantly activated, facilitating malignant tumor development by regulating cancer cell migration and invasion as well as remodeling of the tumor microenvironment (TME) (9,10). In this pathway, TGF-β ligands bind to TGF-β receptor II, phosphorylating TGF-β receptor I (TGF-βRI) and stimulating its serine/threonine kinase activity. Activated TGF-βRI then phosphorylates Smad2 and Smad3, yielding a complex with Smad4 and translocating it to the nucleus to control target gene transcription (11,12). This pathway also influences the transcription of genes associated with epithelial-mesenchymal transition (EMT) (13). Research suggests that TGF-β pathway activation is related to poor prognosis in individuals with LC (14), making it a notable target for LC therapies. The upstream regulatory molecules of the TGF-β pathway in LC are not yet completely understood. Therefore, the present study employed transcriptome sequencing and *in vitro* experiments to identify SLC10A3 as a modulator of the TGF-β pathway, which may facilitate LC progression via altered TGF-β pathway signaling.

Materials and methods

Cell lines and culture. The Thle2 human normal hepatic cell line was acquired from Zhejiang Noble Biological Products Co., Ltd., and the LC cell lines, Huh7 and Hep3B, were purchased from Zishan Biological Company. Cell lines were validated via short tandem repeat profiling. Cells were cultivated in DMEM (Gibco; Thermo Fisher Scientific, Inc.) enriched with 1% penicillin/streptomycin (Pricella; Elabscience Bionovation Inc.) and 10% fetal bovine serum (FBS; Biological Industries; Sartorius AG). The cells were incubated at 37˚C with 5% CO_2 in humidified conditions.

Cell transfection. The synthesis of small interfering RNA (siRNA) that targets the SLC10A3 gene (siSLC10A3) and negative control siRNA (siNC) was conducted by Shanghai GenePharma Co., Ltd. Per the manufacturer's protocols, transfection of siSLC10A3 and siNC (final concentration, 200 nM) was conducted into Huh7 cells via Lipofectamine® 2000 (Invitrogen; Thermo Fisher Scientific, Inc.) or into Hep3B cells via GP Transfect Mate (Shanghai GenePharma Co., Ltd.) at 37˚C. After transfection, the cells were cultured for 36-60 h before conducting subsequent experiments. The transfection procedures were consistent across different culture plates, with reagent amounts adjusted proportionally. The siRNA sequences were as follows (5'-3'): siNC sense, UUCUCCGAA CGUGUCACGUTT and antisense, ACGUGACACGUUCGG AGAATT; Huh7 cells siSLC10A3 sense, CUGACCAUCA AGAACGUGATT and antisense, UCACGUUCUUGAUGG UCAGTT; Hep3B cells siSLC10A3 sense, CUCCAUGAC UUUCCUCUCUTT and antisense, AGAGAGGAAAGUCAU GGAGTT.

RNA extraction and reverse transcription-quantitative PCR (RT-qPCR). After culturing the transfected LC cells in a 6-well plate for 36 h, the cells were washed with phosphate-buffered saline (PBS; Wuhan Servicebio Technology Co., Ltd.). Total RNA isolation was conducted via a tissue/cell RNA isolation kit (cat. no. RN001; ESScience). The RT of isolated RNA into cDNA was conducted via a PrimeScript RT kit (cat. no. RR047A; Takara Bio Inc.) according to the manufacturer's instructions. The qPCR primers were synthesized by Sangon Biotech Co., Ltd. and had the following sequences (5'-3'): SLC10A3 forward CAACAAGTGTTCGTTTGGGTG and reverse CCATGAGGAAAGCGTACAAGG; GAPDH forward CAGGAGGCATTGCTGATGAT and reverse GAA GGCTGGGGCTCATTT; cyclin D1 forward ATCAAGTGT GACCCGGACTG and reverse CTTGGGGTCCATGTTCTG CT; p21 forward GCTGCCGAAGTCAGTTCCTT and reverse TTCTGACATGGCGCCTCC. qPCR reactions were conducted utilizing TB Green Premix Ex Taq II (cat. no. RR820A; Takara Bio Inc.) with the CFX Duet real-time PCR system (Thermo Fisher Scientific, Inc.). The qPCR reaction protocol began with an initial denaturation step (95˚C, 30 sec) and then 40 cycles of denaturation (95˚C, 5 sec) and annealing (60˚C, 30 sec). The $2^{-\Delta\Delta Cq}$ method was utilized to assess the relative levels of the genes, using GAPDH as an internal control (15).

Western blot (WB) analysis. LC cells transfected in a 6-well plate were cultured for 60 h, then washed with PBS. Cell lysis was conducted using RIPA buffer (cat. no. R0010; Beijing Solarbio Science & Technology Co., Ltd.) supplemented with 1% protease inhibitor (cat. no. FJP0100; Beijing Solarbio Science & Technology Co., Ltd.) and 1% phosphatase inhibitor (cat. no. HY-K0021; MedChemExpress). The supernatant was collected and centrifuged at 13,000 x g for 20 min at 4˚C. Protein levels were assessed using the BCA protein assay kit (cat. no. PC0020; Beijing Solarbio Science & Technology Co., Ltd.). The separation of protein samples (30 μg each lane) was conducted by 10% SDS-PAGE, which were then transferred onto a PVDF membrane (cat. no. IPVH00010; MilliporeSigma; Merck KGaA). The membrane was blocked with a protein-free rapid blocking solution (cat. no. PS108P; Epizyme; Ipsen Pharma) for 15 min at room temperature. Next, primary antibodies were applied at an appropriate ratio in universal antibody diluent (cat. no. PS119L; Epizyme; Ipsen Pharma) and incubated overnight at 4˚C. The primary antibodies utilized were as follows: GAPDH (1:3,000; cat. no. AB-P-R 001; Hangzhou Goodhere Biotechnology Co. Ltd.), SLC10A3 (1:1,000; cat. no. 19909-1-AP; Proteintech Group, Inc.), phosphorylated (p-)Smad2 (Ser465 + 467; 1:1,000; cat. no. PT0662R; ImmunoWay Biotechnology), Smad2 (1:1,000; cat. no. F0309; Selleck Chemicals), p-Smad3 (Ser423 + 425; 1:2,000; cat. no. F2846; Selleck Chemicals), Smad3 (1:1,000; cat. no. F0364; Selleck Chemicals), epithelial cadherin (E-Cadherin; 1:1,000; cat. no. F0005; Selleck Chemicals) and vimentin (1:3,000; cat. no. bs-8533R; BIOSS). The next day, the membrane was incubated with an HRP-conjugated secondary antibody (1:6,500; cat. no. RGAR001; Proteintech Group, Inc.) at 37˚C for 1 h. Lastly, protein bands were observed via the ChemiDoc XRS+ gel imaging system (ECL; Bio-Rad Laboratories, Inc.), and band density was quantified using ImageJ software (version 1.53; National Institutes of Health).

Enzyme-linked immunosorbent assay (ELISA). Human TGF-β1 secretion into the supernatant by LC cells with SLC10A3 knockdown was detected using a commercial human TGF-β1 ELISA kit (cat. no. ml022522; Shanghai Enzyme-linked Biotechnology Co., Ltd.). Briefly, cells were cultured with serum-free medium, then cell culture

supernatants were collected and centrifuged at 300 x g for 5 min at 4˚C to remove cell debris. Subsequent ELISA procedures were performed strictly according to the manufacturer's instructions. The absorbance value of each well was measured at 450 nm using a microplate reader. The concentration of TGF-β1 in each sample was calculated based on a standard curve.

Transcriptome sequencing and bioinformatics analysis. Hep3B and Huh7 cells transfected with siSLC10A3 or siNC were cultured in 6-well plates for 36 h. Three independent biological replicates were included in each group, yielding a total of 12 samples. Total RNA was extracted using Total RNA Extractor (cat. no. B511311; Sangon Biotech Co., Ltd.) according to the manufacturer's instructions. RNA concentration was measured using a Qubit 2.0 fluorometer (Invitrogen; Thermo Fisher Scientific, Inc.) with a Qubit 2.0 RNA assay kit (cat. no. Q32855; Thermo Fisher Scientific, Inc.). RNA integrity was assessed using an Agilent RNA bioanalysis system (Agilent Technologies), and the RNA integrity number ranged from 9.9 to 10.0.

RNA library preparation and sequencing were performed by Sangon Biotech Co., Ltd. Sequencing libraries were prepared using the Hieff NGS Ultima Dual-mode mRNA Library Prep Kit [cat. no. 12309; Yeasen Biotechnology (Shanghai) Co., Ltd.] according to the manufacturer's instructions. Briefly, poly(A)-containing mRNA was enriched from total RNA using oligo(dT) magnetic beads and subsequently fragmented. The fragmented mRNA was reverse-transcribed into first-strand cDNA, followed by second-strand cDNA synthesis, end repair, dA-tailing, adapter ligation, purification, size selection and PCR amplification. Library concentration and fragment size were evaluated before sequencing. The qualified libraries were sequenced on the DNBSEQ-T7 platform (MGI Tech Co., Ltd.) using a paired-end 150-bp sequencing strategy.

Raw sequencing data were evaluated using FastQC (https://www.bioinformatics.babraham.ac.uk/projects/fastqc/), and adapter sequences and low-quality reads were removed using fastp (https://github.com/OpenGene/fastp) to obtain clean reads. The quality-controlled reads were aligned to the human reference genome using HISAT2 (https://github.com/DaehwanKimLab/hisat2), and alignment statistics were evaluated using RSeQC (https://rseqc.sourceforge.net/). Transcript abundance was quantified in transcripts per million (TPM) using StringTie (https://ccb.jhu.edu/software/stringtie/). Differential expression analysis was conducted using DESeq2 (https://bioconductor.org/packages/DESeq2/). Differentially expressed genes (DEGs) were identified using the criteria of an adjusted P-value (q-value) <0.05 and $|\log_2$ fold-change (FC)| >0.5. Gene Ontology (GO) and Kyoto Encyclopedia of Genes and Genomes (KEGG) enrichment analyses were performed to investigate the biological functions and pathways associated with the DEGs.

Cell Counting Kit-8 (CCK-8) assay. Hep3B and Huh7 cells were grown ($1x10^3$ cells/well) in 96-well plates. A 10% CCK-8 solution (cat. no. C6005; Suzhou Xinsaimei Biotechnology Co., Ltd.) was applied to each well following 24, 48, 72 and 96 h of incubation. Following a further 2 h of incubation, the absorbance at 450 nm was measured via a Thermo Fisher Scientific, Inc. enzyme-linked immunosorbent assay reader.

5-ethynyl-2'-deoxyuridine (EdU) assay. Cell growth was estimated via the BeyoClick™ EdU-555 Cell Proliferation Kit (cat. no. C0075S; Beyotime Biotechnology) as per the manufacturer's guidelines. Hep3B and Huh7 cells were seeded ($1.3x10^5$ cells/well) in a 12-well plate. After culturing for 24 h, 10 μM EdU was incubated with the samples for an additional 2 h. The cells were fixed with 4% paraformaldehyde (Beijing Solarbio Science & Technology Co., Ltd.) for 15 min at room temperature (20-25˚C), permeabilized using 0.5% Triton X-100 immunostaining permeabilization solution (Beyotime Biotechnology) for another 15 min at room temperature and then incubated with the Click reaction solution in the dark for 30 min at room temperature. Hoechst 33342 was utilized to stain the cell nuclei for 10 min at room temperature. Images were obtained via a Leica fluorescence microscope, and the EdU positivity rate was assessed by the division of the number of EdU-positive cells by the total number of Hoechst 33342-stained cells, facilitating the assessment of cell proliferation capacity.

Colony formation assay. The cells ($5x10^3$/well) were seeded in a 6-well plate and incubated for 14 days. After culturing for 14 days, the cells were fixed with 4% paraformaldehyde (Beijing Solarbio Science & Technology Co., Ltd.) for 15 min at room temperature and stained with 0.1% crystal violet (Beyotime Biotechnology) for another 15 min at room temperature. After three PBS washes, images were taken and the colonies were counted. A colony was defined as a cell cluster containing ≥30 cells. Colony quantification was performed using ImageJ software (version 1.53; National Institutes of Health).

Wound healing assay. LC cells in the logarithmic growth phase were cultured in a 6-well plate for 24 h before transfection. After an additional 48 h, a scratch was created via a 200 μl pipette tip when the cells reached 90-100% confluence. The wells were washed with PBS thrice before adding serum-free DMEM. Images were taken using a phase contrast inverted microscope (Leica Microsystems GmbH) at 0 and 24 h post-scratch to examine the wound closure. The wound closure area was quantified using ImageJ software (version 1.53; National Institutes of Health). The wound boundaries were outlined to calculate the closure area. The changes in the area of the scratches were calculated and analyzed.

Transwell invasion assay. Matrigel (ABW; cat. no. 0827045; Nova Biotechnology) was diluted in serum-free culture medium (1:8 ratio) and then used to coat the top chamber of a Transwell plate (Wuhan NEST Biotechnology Co., Ltd.). The plate was incubated at 37˚C for 2 h to facilitate gel formation. A total of 700 μl complete culture medium containing 15% FBS was added to the bottom chamber to serve as a chemotactic agent. To assess cell invasion, $5x10^4$ cells diluted in 200 μl of serum-free culture medium were applied to the top Transwell chamber. After a 48-h incubation at 37˚C in a 5% CO_2 environment, the non-invading cells on the upper membrane surface were eliminated. The invaded cells on the bottom membrane surface underwent fixing with 4% paraformaldehyde at

room temperature for 20 min and staining with 0.1% crystal violet at room temperature for 20 min. In total, five random fields of view were captured using a phase contrast inverted microscope, and ImageJ (version 1.54d; National Institutes of Health) was utilized for the quantification of invaded cells.

Tumor Immune Estimation Resource 2.0 (TIMER2), Gene Expression Profiling Interactive Analysis 2 (GEPIA2) and The Cancer Genome Atlas (TCGA). The expression profile of SLC10A3 across various cancer types was analyzed using data from TIMER2 (http://timer.comp-genomics.org/). SLC10A3 expression levels in LC were examined via GEPIA2 (http://gepia2.cancer-pku.cn/). DEGs with the $P<0.05$ and $|\log_2FC| >0.5$ criteria were observed. Survival data for SLC10A3 in individuals with LC were obtained from the TCGA (https://cancergenome.nih.gov). Kaplan-Meier survival analysis was performed to evaluate the prognostic significance of SLC10A3 expression in patients with liver hepatocellular carcinoma (LIHC). RNA-sequencing data and corresponding clinical information were obtained from The Cancer Genome Atlas (TCGA) using the TCGAbiolinks R package. Patients with available primary tumor expression data and valid overall survival information were included in the analysis. SLC10A3 expression levels were quantified in TPM and transformed as log2(TPM + 1). The optimal cut-off value was determined using maximally selected rank statistics implemented in the surv_cutpoint function of the R package survminer, with a minimum group proportion of 0.10. The resulting cut-off value was 4.868588 [log2(TPM + 1)], equivalent to 28.214 TPM. Patients were classified into high-expression (n=62) and low-expression (n=306) groups based on this threshold. Overall survival was calculated using the recorded time to death or last follow-up. Survival curves were generated using the Kaplan-Meier method, and differences between groups were assessed using the log-rank test. Hazard ratios and 95% confidence intervals were calculated using univariable Cox proportional hazards regression.

Statistical analysis. GraphPad Prism 10.1.2 (Dotmatics) was utilized for data analysis, and the results are presented as the mean ± standard deviation. Unpaired Student's t-test was utilized for two-group comparisons, whereas one-way analysis of variance and then Tukey's post hoc test were utilized for comparisons between several groups. Experiments were conducted at least three times independently. $P<0.05$ was considered to indicate a statistically significant difference.

Results

SLC10A3 is upregulated in LC tissues and is associated with poor prognosis. Prior investigations have shown that SLC10A3 is key in the onset and development of multiple tumor types. In line with this, analysis using the TIMER2 database illustrated that SLC10A3 was upregulated in numerous tumor types, including LC (Fig. 1A). The GEPIA2 database was utilized to analyze the SLC10A3 expression levels in LC tissues, aiming to examine its function and clinical relevance in LC progression. The GEPIA2 LIHC cohort included 369 tumor and 160 normal samples for expression comparison between tumor and normal tissues. Compared with normal liver tissues, a significant upregulation of SLC10A3 in LC tissues was observed (Fig. 1B; $P<0.05$). To further investigate the prognostic significance of SLC10A3 expression, transcriptomic and clinical data from the TCGA-LIHC cohort were analyzed. A total of 368 patients with available primary tumor gene expression data and valid overall survival information were included. The patients ranged in age from 16.0 to 87.9 years, with a median age of 61.9 years. Among them, 240 (65.2%) were male and 128 (34.8%) were female. Histologically, 357 patients (97.0%) had hepatocellular carcinoma, 4 (1.1%) had fibrolamellar hepatocellular carcinoma, 6 (1.6%) had combined hepatocellular-cholangiocarcinoma and 1 (0.3%) was classified as other/unclassified. The results illustrated that elevated SLC10A3 expression was related to a significantly reduced overall survival compared with SLC10A3 downregulation (Fig. 1C; $P<0.001$).

SLC10A3 expression characteristics in LC cell lines and verification of the knockdown efficiency of siSLC10A3. WB analysis illustrated a significant elevation in SLC10A3 protein levels in Hep3B and Huh7 LC cell lines compared with the normal Thle2 liver cell line (Fig. 2A and B; $P<0.001$). The role of SLC10A3 in LC was investigated by transfecting LC cells with siSLC10A3 to reduce its expression. Knockdown efficiency was evaluated by analyzing SLC10A3 expression changes at the mRNA level using RT-qPCR and at the protein level using WB analysis. The outcomes illustrated that the SLC10A3 level was significantly lowered in cells transfected with siSLC10A3 compared with siNC (Fig. 2C-E; all $P<0.0001$). The successful transfection of siSLC10A3 yielded a significant decrease in SLC10A3 expression levels in LC cells.

Impact of knocking down SLC10A3 expression on the transcriptome of LC cells: Sequencing data quality control and differential expression analysis. Transcriptome sequencing and quality control of the siNC and siSLC10A3 groups (n=3 per group) was conducted for both Hep3B and Huh7 cells. The results showed that all samples had percentage of bases with sequencing quality scores >20 scores >99% and percentage of bases with sequencing quality scores >30 scores >96%, confirming high sequencing quality and data reliability (Tables I and II). Principal component analysis indicated that the cumulative variance explained by PC1 (68.32%) and PC2 (15.68%) reached 84%, with no overlap between the groups and a clear separation trend observed. This suggested that the knockdown of SLC10A3 expression markedly altered the overall transcriptional expression profile of the cells, indicating a regulatory role of SLC10A3 in the cell transcriptome (Fig. 3A). The sequencing data from the siNC and siSLC10A3 groups were analyzed using DESeq to obtain the FC values, with screening criteria set at $q<0.05$ and $|\log2FC| >0.5$. This analysis resulted in the identification of 1,400 DEGs in Hep3B cells, including 571 upregulated and 829 downregulated genes (Fig. 3B). In Huh7 cells, 485 DEGs were identified, comprising 172 upregulated and 313 downregulated genes (Fig 3C). Clustering analysis of the two DEG sets revealed notable differences between the siNC and siSLC10A3 groups (Fig. 3D), further confirming that the knockdown of SLC10A3 extensively regulated gene expression levels in LC cells.

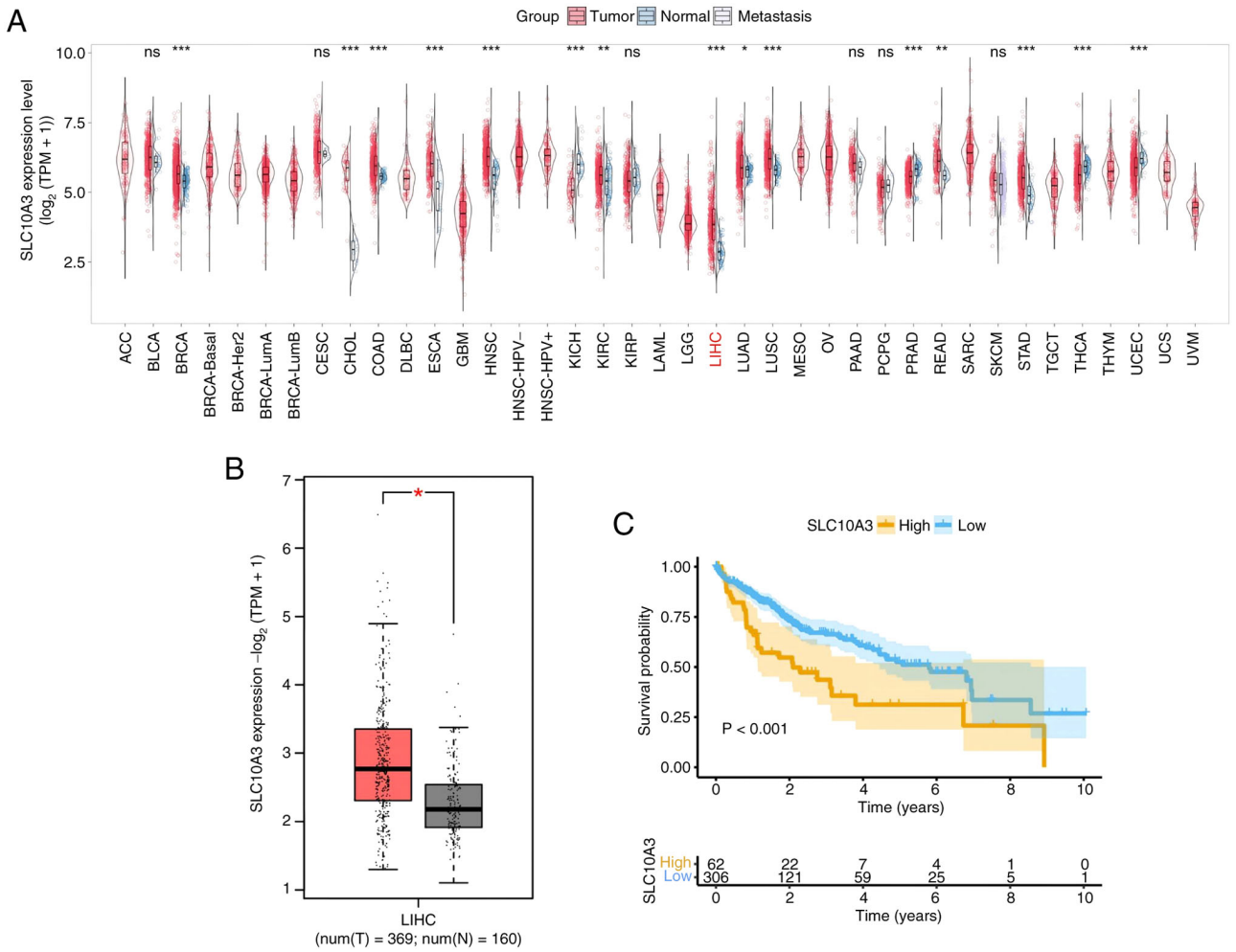


Figure 1. SLC10A3 is elevated in liver cancer and is associated with poor patient prognosis. (A) Analysis of SLC10A3 expression across numerous cancer types. (B) Comparison of the SLC10A3 levels in LC tissues (tumor; red) vs. neighboring non-cancerous tissues (normal; gray). (C) Kaplan-Meier survival analysis according to the SLC10A3 level. *P<0.05, **P<0.01, ***P<0.001. SLC10A3, solute carrier family 10 member 3; TPM, transcripts per million; ns, not significant; LIHC, liver hepatocellular carcinoma.

Functional enrichment analysis was conducted on DEGs in LC cells following the knockdown of SLC10A3. KEGG analysis was conducted on the DEGs from the siNC and siSLC10A3 groups to explore the related signaling pathways. The analysis identified 10 pathways that were significantly enriched in both cell types (P<0.05). These pathways encompassed the 'Complement and coagulation cascades', 'Alanine, aspartate and glutamate metabolism', 'Glycine, serine and threonine metabolism', 'PPAR signaling pathway' 'TGF-β signaling pathway', 'Cholesterol metabolism', 'Pyruvate metabolism', 'Drug metabolism - cytochrome P450', 'Chemical carcinogenesis-DNA adducts' and 'Metabolism of xenobiotics by cytochrome P450' (Fig. 4A and B). GO analysis was performed to investigate the functional characteristics of the DEGs in terms of cellular component, biological process and molecular function. When sorting the outcomes based on q-values and retaining the top five entries in each category (Fig. 4C and D), it was found that the DEGs in both types of LC cells were predominantly enriched in metabolic regulation, intercellular communication (specifically related to extracellular vesicles/exosomes), signal molecule interactions and enzyme activity regulation. These functional characteristics closely align with the core regulatory roles of the TGF-β signaling pathway, including metabolic reprogramming, signal transduction, TME remodeling and the regulation of invasion and metastasis. The results of the KEGG and GO enrichment analyses suggested that SLC10A3 may influence LC progression by controlling the TGF-β pathway.

SLC10A3 knockdown suppresses TGF-β pathway signaling in LC cells. The association between SLC10A3 and the TGF-β pathway was explored using WB analysis to assess changes in the abundance of key proteins. The findings revealed that SLC10A3 knockdown in LC cells significantly reduced the p-Smad2/total Smad2 and p-Smad3/total Smad3 ratios (Fig. 5A-C; P<0.01). Additionally, ELISA results revealed that TGF-β1 secretion was significantly suppressed in the siSLC10A3 group relative to the siNC group (Fig. 5F; P<0.01). Specifically, SLC10A3 knockdown was observed to reduce TGF-β1 secretion, accompanied by decreased Smad2/3 phosphorylation and attenuated TGF-β pathway signaling. These findings suggest that SLC10A3 may be associated with modulation of the TGF-β pathway.

Table I. Statistics of quality control data for Hep3B cell samples.

Group	Sample	Total bases count, bp	Q20 bases count, bp	Q20 bases ratio, %	Q30 bases count, bp	Q30 bases ratio, %
Control	siNC-1	6,324,857,967	6,278,968,423	99.27	6,158,884,507	97.38
Control	siNC-2	5,482,306,394	5,444,663,294	99.31	5,345,178,623	97.5
Control	siNC-3	6,015,230,216	5,970,881,975	99.26	5,854,123,382	97.32
Knock down	siSLC10A3-1	5,695,123,017	5,653,514,508	99.27	5,543,485,425	97.34
Knock down	siSLC10A3-2	5,545,552,919	5,505,681,303	99.28	5,399,681,643	97.37
Knock down	siSLC10A3-3	5,475,499,011	5,436,783,564	99.29	5,334,071,081	97.42

Q20, percentage of bases with sequencing quality scores >20; Q30, percentage of bases with sequencing quality scores >30, bp; base pair, si; small interfering RNA; NC, negative control; SLC10A3, solute carrier family 10 member 3.

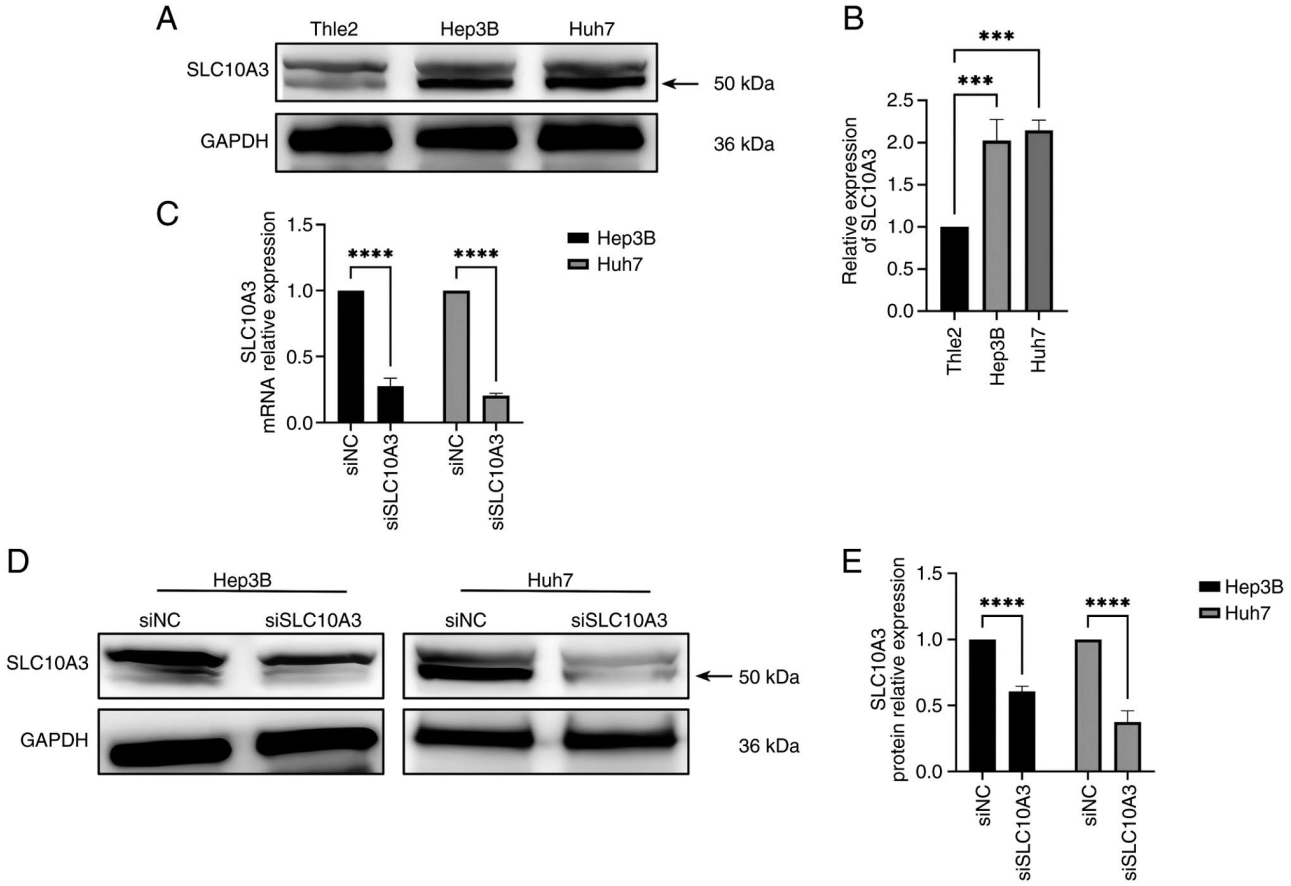


Figure 2. SLC10A3 expression characteristics and validation of siSLC10A3 knockdown efficiency in LC cell lines. (A) Western blotting detection of endogenous SLC10A3 protein in Thle2, Hep3B and Huh7 cells. (B) Densitometric quantification of endogenous SLC10A3 protein levels from the western blotting results shown in (A). (C) RT-qPCR assessment of siSLC10A3 knockdown efficiency at the mRNA level in Hep3B and Huh7 cells. (D) Western blotting detection of SLC10A3 protein after siSLC10A3 transfection in Hep3B and Huh7 cells. (E) Densitometric quantification of SLC10A3 protein levels from the western blotting results shown in (D). ***P<0.001, ****P<0.0001 vs. siNC. si, small interfering RNA; NC, negative control; SLC10A3, solute carrier family 10 member 3.

TGF-β has a key function in EMT, a major process in tumor metastasis and invasion (16,17). Therefore, EMT-related molecules downstream of the TGF-β pathway were assessed. The results showed upregulation of E-cadherin and downregulation of vimentin (Fig. 5A, D and E). The findings suggested that SLC10A3 knockdown may reverse the EMT process in LC cells by suppressing TGF-β pathway signaling.

Knockdown of SLC10A3 inhibits the proliferative ability of LC cells. Next, the role of SLC10A3 was explored through various cell proliferation assays. The effects of siNC and siSLC10A3 on the proliferation of Hep3B and Huh7 cells were assessed using a CCK-8 assay. The outcomes illustrated that SLC10A3 suppression significantly reduced the proliferation of LC cells (Fig. 6A; P<0.001). The suppression of SLC10A3 expression also yielded a marked decline in the colony formation capability

Table II. Statistics of quality control data for Huh7 cell samples.

Group	Sample	Total bases count, bp	Q20 bases count, bp	Q20 bases ratio, %	Q30 bases count, bp	Q30 bases ratio, %
Control	siNC-1	5,308,675,560	5,271,637,844	99.3	5,173,183,456	97.45
Control	siNC-2	5,996,614,403	5,952,056,734	99.26	5,832,599,108	97.26
Control	siNC-3	6,182,377,596	6,130,904,318	99.17	5,996,209,858	96.99
Knock-down	siSLC10A3-1	6,334,389,771	6,289,484,471	99.29	6,169,195,581	97.39
Knock-down	siSLC10A3-2	6,403,497,238	6,350,880,863	99.18	6,215,377,075	97.06
Knock-down	siSLC10A3-3	6,260,202,443	6,214,229,784	99.27	6,094,833,665	97.36

Q20, percentage of bases with sequencing quality scores >20; Q30, percentage of bases with sequencing quality scores >30, bp; base pair, si; small interfering RNA; NC, negative control; SLC10A3, solute carrier family 10 member 3.

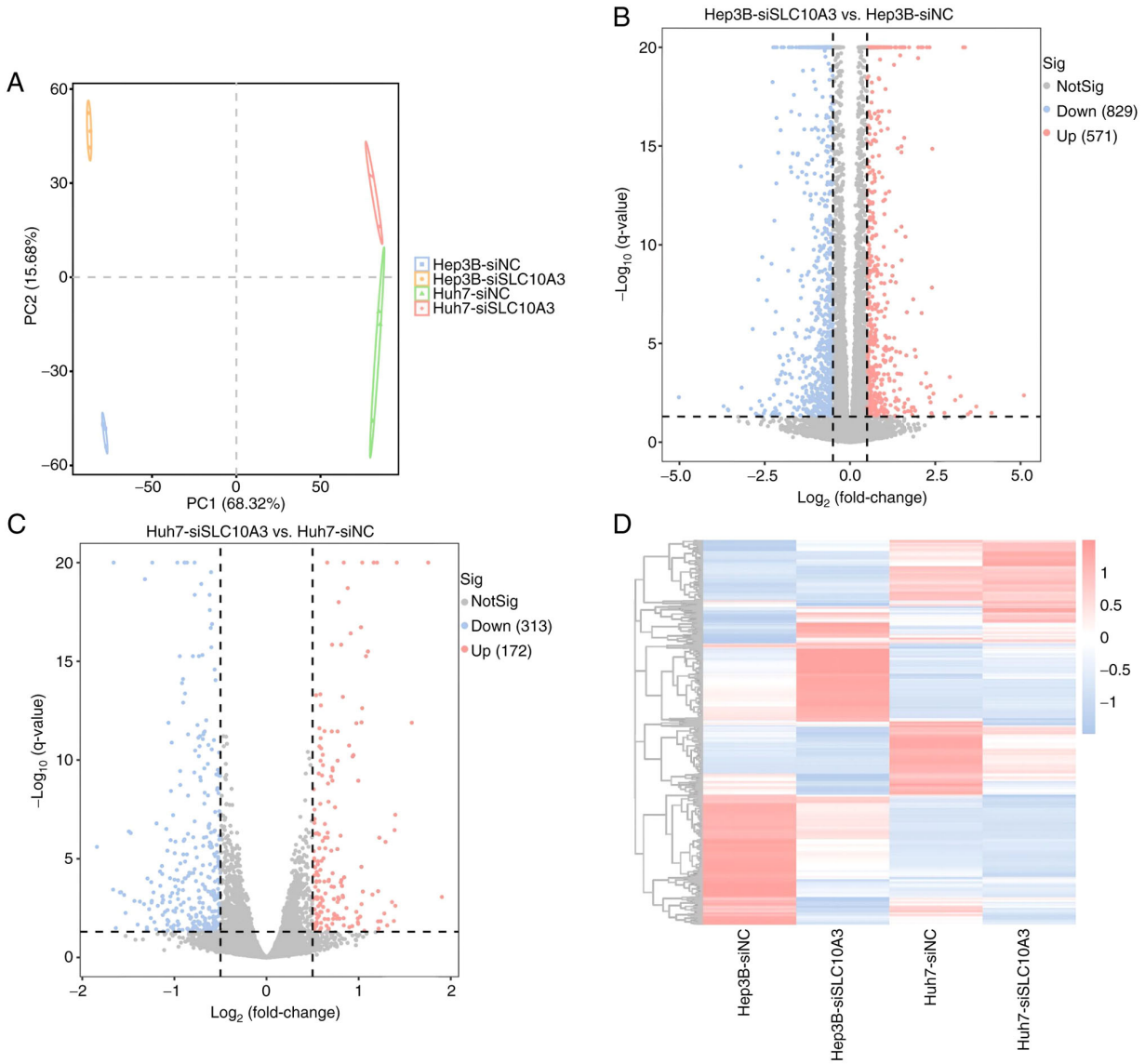


Figure 3. Overall characteristics and distribution of the DEGs from the transcriptome sequencing data of liver cancer cells with SLC10A3 knockdown. (A) Principal component analysis plot. Volcano plots of the DEGs in (B) Hep3B and (C) Huh7 cells. (D) Clustering heatmap of the DEGs. DEGs, differentially expressed genes; SLC10A3, solute carrier family 10 member 3; si, small interfering RNA; NC, negative control; up, upregulated; down, downregulated.

of LC cell lines (Fig. 6B and D; P<0.0001). The EdU assay was performed to assess the levels of newly synthesized DNA. The results indicated that reducing SLC10A3 expression notably inhibited LC cell proliferation (Fig. 6C, E and F; P<0.0001).

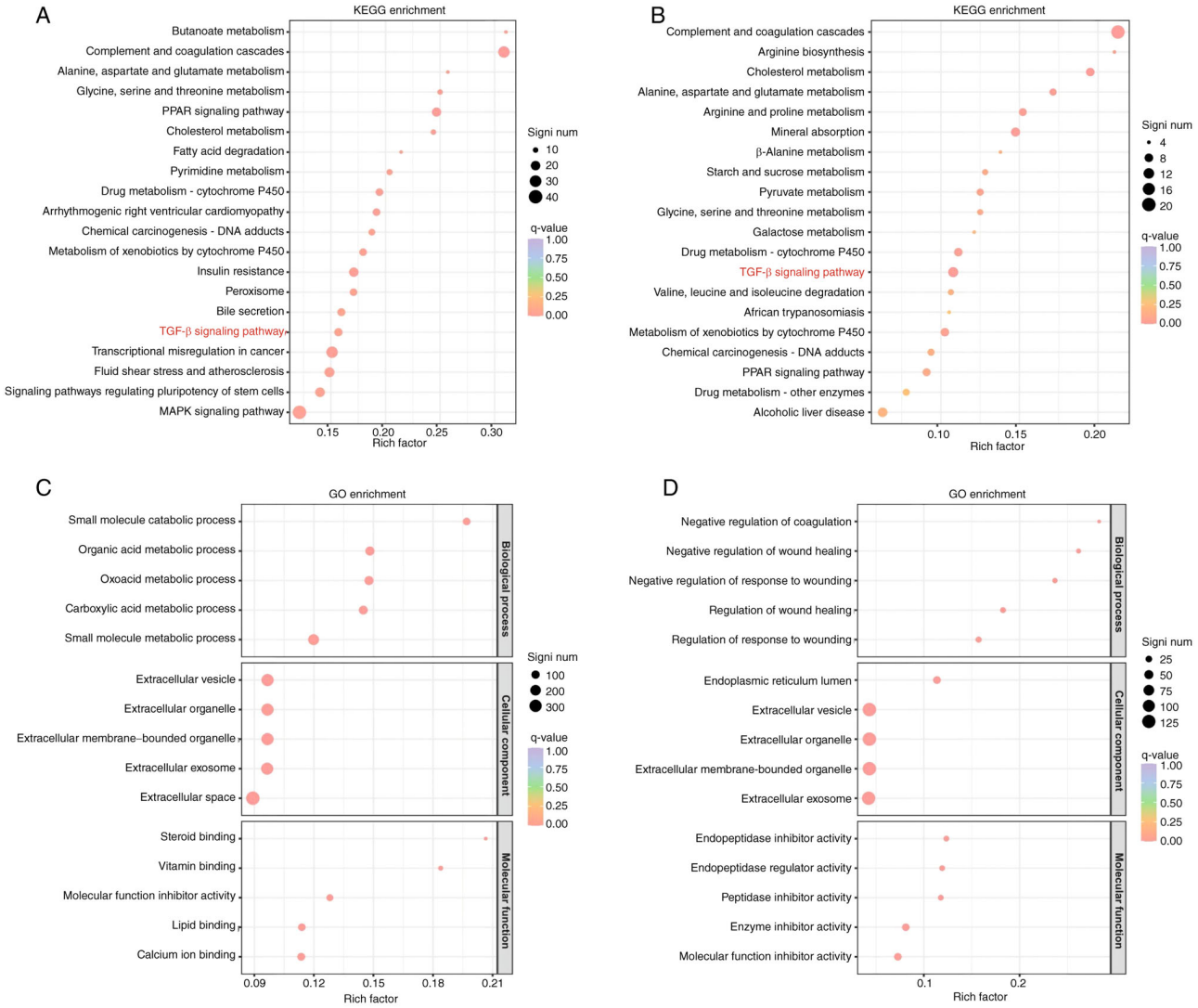


Figure 4. Functional enrichment analysis of the DEGs in LC cells with SLC10A3 knockdown. (A) KEGG analysis for the DEGs in Hep3B cells. (B) KEGG analysis for the DEGs in Huh7 cells. (C) GO analysis for the DEGs in Hep3B cells. (D) GO analysis for the DEGs in Huh7 cells. DEGs, differentially expressed genes; KEGG, Kyoto Encyclopedia of Genes and Genomes; SLC10A3, solute carrier family 10 member 3; GO, Gene Ontology; PPAR, peroxisome proliferator-activated receptor; Signi num, number of significantly enriched genes.

To further elucidate the potential molecular mechanisms underlying the observed inhibition of cell proliferation, RT-qPCR was performed to evaluate the expression levels of the key cell cycle regulatory factors, cyclin D1 and p21. The results showed that, compared with the siNC group, the expression level of Cyclin D1 was significantly downregulated in the siSLC10A3 group, while the level of the cell cycle inhibitory gene p21 was significantly upregulated (Fig. 6G; P<0.01). These results demonstrate that knockdown of SLC10A3 induces cell cycle arrest by regulating cyclin D1 and p21 expression, thereby suppressing cell proliferation.

Exogenous TGF-β1 can rescue the suppression of TGF-β pathway signaling induced by SLC10A3 knockdown. WB analysis was performed to assess the protein levels of key markers in the siSLC10A3 group and the siSLC10A3 combined with TGF-β1 (10 ng/ml; siSLC10A3 + TGF-β1) group, to explore whether exogenous TGF-β1 could restore TGF-β pathway signaling following SLC10A3 knockdown. The results indicated a significant elevation in the p-Smad2/Smad2 and p-Smad3/Smad3 ratios in the siSLC10A3 + TGF-β1 group compared with the siSLC10A3 group (Fig. 7; P<0.05). The present finding indicated that exogenous TGF-β1 effectively restored Smad2/3 phosphorylation in SLC10A3-knockdown cells and recovered TGF-β pathway signaling.

SLC10A3 improves the migratory and invasive capacities of LC cells via modulation of the TGF-β pathway signaling. Due to the important impact of the invasion and metastasis of tumor cells on the progression of cancer and patient outcomes (18), the influence of SLC10A3 on the ability of LC cells to migrate and invade were examined through wound healing and Transwell invasion assays. In the wound healing assay, suppression of SLC10A3 expression significantly decreased the migration of Hep3B and Huh7 cells (Fig. 8A and B; P<0.05). Notably, the TGF-β pathway activator TGF-β1 reversed this inhibitory effect. In the Transwell invasion assay, siSLC10A3 significantly lowered the invasive ability of LC cells compared with the control (P<0.001), a reduction that was reversed by TGF-β1 (Fig. 8C-E). These findings suggest that SLC10A3 may

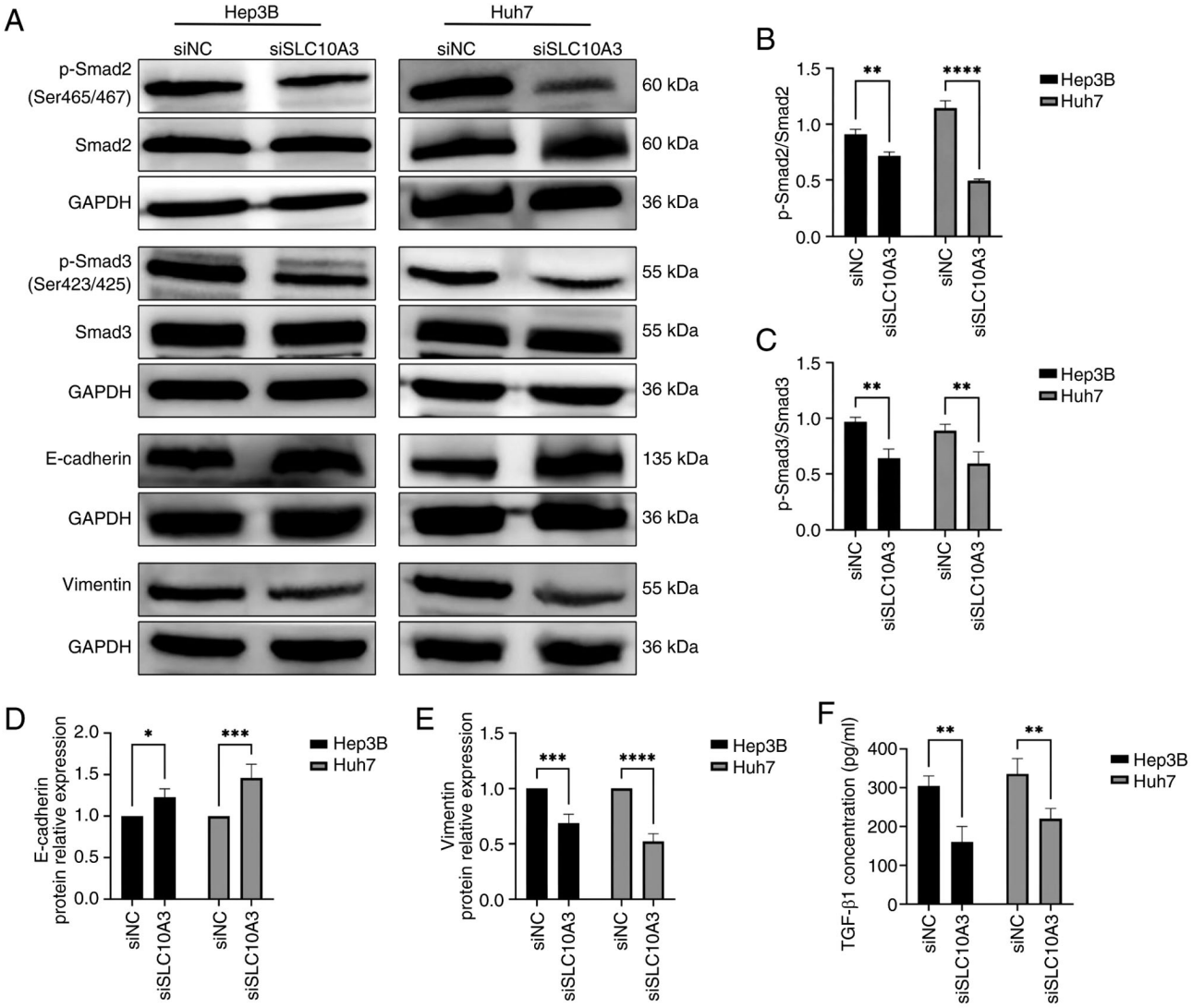


Figure 5. Effects of SLC10A3 knockdown on key markers of the TGF-β signaling pathway. (A) Western blot analysis of core proteins in the TGF-β pathway (p-Smad2, Smad2, p-Smad3 and Smad3) and epithelial-mesenchymal transition-related proteins (E-cadherin and vimentin) following SLC10A3 knockdown. Semi-quantitative analysis of (B) p-Smad2/Smad2, (C) p-Smad3/Smad3, (D) E-cadherin and (E) vimentin protein levels following SLC10A3 knockdown. (F) Effect of SLC10A3 knockdown on TGF-β1 secretion in liver cancer cells. *P<0.05, **P<0.01, ***P<0.001, ****P<0.0001 vs. siNC. si, small interfering RNA; TGF-β, transforming growth factor-β; NC, negative control; p-, phosphorylated; SLC10A3, solute carrier family 10 member 3; E-cadherin, epithelial cadherin.

enhance the migratory and invasive capacities of LC cells via modulation of TGF-β pathway signaling.

Discussion

LC is a heterogeneous malignant tumor with complex biological features that hamper early detection and result in poor clinical outcomes (19,20), imposing a heavy burden on the global healthcare system. Despite advances in diagnosis and treatment, patients with advanced LC still have a poor prognosis (21), making it urgent to explore novel molecular targets for targeted therapy.

As a unique member of solute carrier family 10, SLC10A3 primarily mediates the transport of steroid hormones and bile acids, and is generally regarded as a housekeeping protein with largely undefined biological functions (22). Existing studies have confirmed the oncogenic role of SLC10A3 in multiple solid tumor types, including glioblastoma (23), colorectal cancer (7) and head and neck cancer (24). Consistent with bioinformatics predictions, the results of the present study verified the upregulation of SLC10A3 in LC and its association with poor prognosis, implying its potential value as a novel prognostic biomarker and mechanistic research candidate.

Multiple signaling pathways jointly dominate LC initiation and progression. Dysregulation of the Wnt/β-catenin, TGF-β and PI3K/AKT/mTOR pathways participates extensively in tumorigenesis, metabolic reprogramming, EMT and TME remodeling (2,25-28). EMT is governed by multiple cascades, drives tumor invasion and metastasis and is accompanied by the altered expression of epithelial and mesenchymal markers (29,30). Tumor cell metabolic reprogramming rewires nutrient uptake to sustain rapid proliferation (31,32). The TME, which is composed of tumor, stromal and immune cells (33), induces metabolic reprogramming and nutrient competition, further modulating tumor immune escape and malignant progression (34).

In the present study, based on transcriptome sequencing and enrichment analyses, the TGF-β signaling pathway was

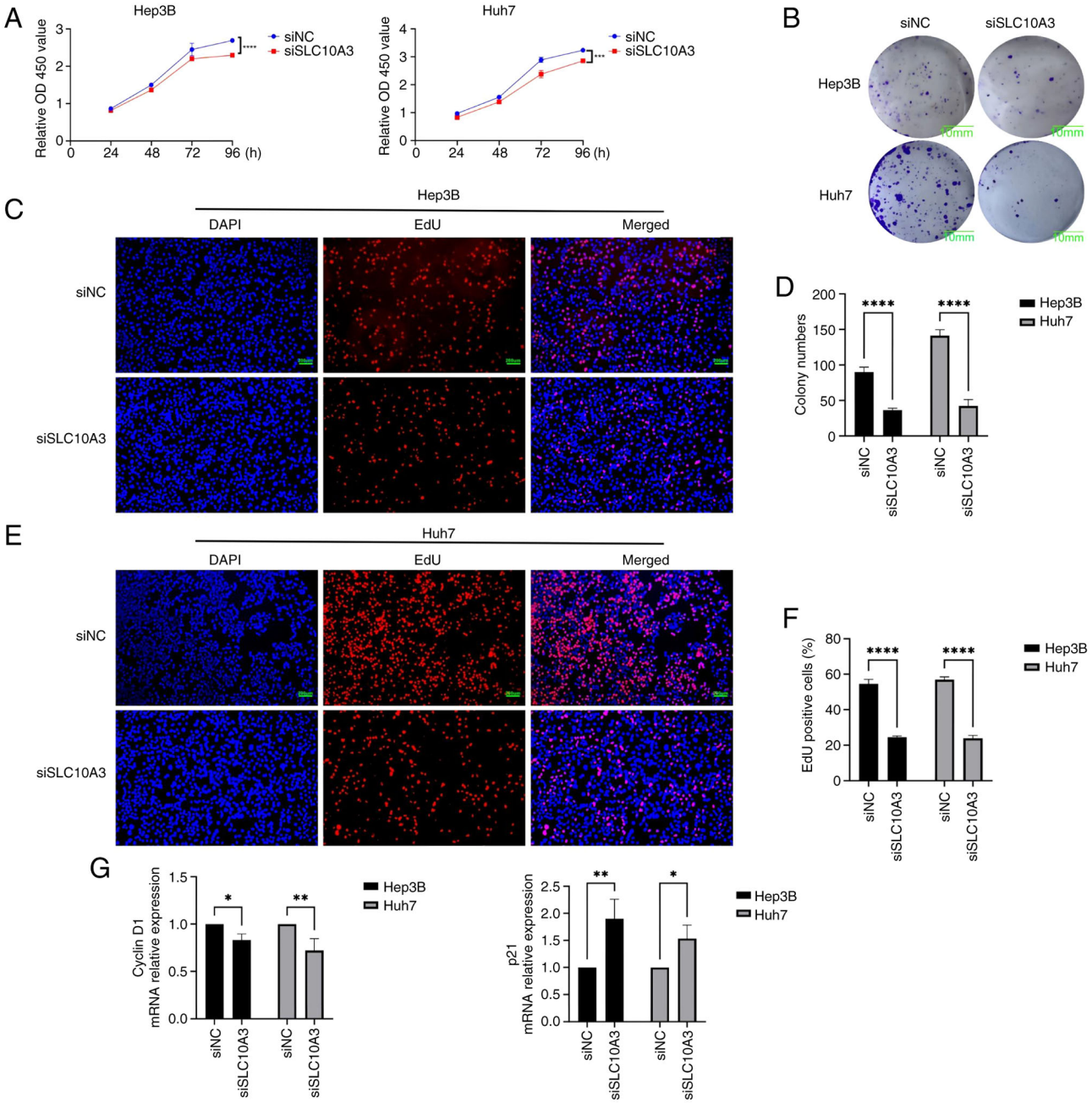


Figure 6. Influence of SLC10A3 knockdown on the proliferative ability of LC cells. (A) Cell Counting Kit-8 assays were utilized to estimate the influence of SLC10A3 knockdown on LC cell viability. (B) Plate colony formation assays were performed to visualize the colony-forming phenotypes of Hep3B and Huh7 cells following SLC10A3 knockdown. (C) EdU fluorescence images showing the proliferative status of Hep3B cells after SLC10A3 knockdown (magnification, ×100; scale bar, 200 μm). (D) Statistical quantification of colony numbers corresponding to the colony formation images shown in (B). (E) EdU fluorescence images showing the proliferative status of Huh7 cells after SLC10A3 knockdown (magnification, x100; scale bar, 200 μm). (F) Statistical analysis of EdU-positive cell ratios quantified from the EdU fluorescence images presented in (C) and (E). (G) Reverse transcription-quantitative PCR was used to evaluate the expression levels of key cell cycle regulatory factors. *P<0.05, **P<0.01, ***P<0.001, ****P<0.0001 vs. siNC. si, small interfering RNA; NC, negative control; SLC10A3, solute carrier family 10 member 3; LC, liver cancer; EdU, 5-ethynyl-2'-deoxyuridine.

identified as one key pathway whose activity is altered by SLC10A3. As a multifunctional cytokine, TGF-β exerts dual roles in LC in a stage-dependent manner; it suppresses proliferation at early tumor stages but promotes EMT and metastasis during malignant progression (35-37). The mechanistic investigation performed in the present study further indicated that SLC10A3 may modulate Smad2/3 phosphorylation and alter TGF-β pathway signaling. Furthermore, exogenous TGF-β1 intervention rescued the phenotypic changes caused by SLC10A3 knockdown, supporting the association between SLC10A3 and the TGF-β pathway.

EMT phenotypic transition endows LC cells with invasive and metastatic properties, characterized by the dysregulated expression of epithelial and mesenchymal biomarkers (38,39). TGF-β, a key EMT driver, promotes tumor metastasis (40). In line with a previous report on cancer-related genes in LC (41), the results of the present study indicated that SLC10A3 may promote EMT progression via modulation of TGF-β pathway

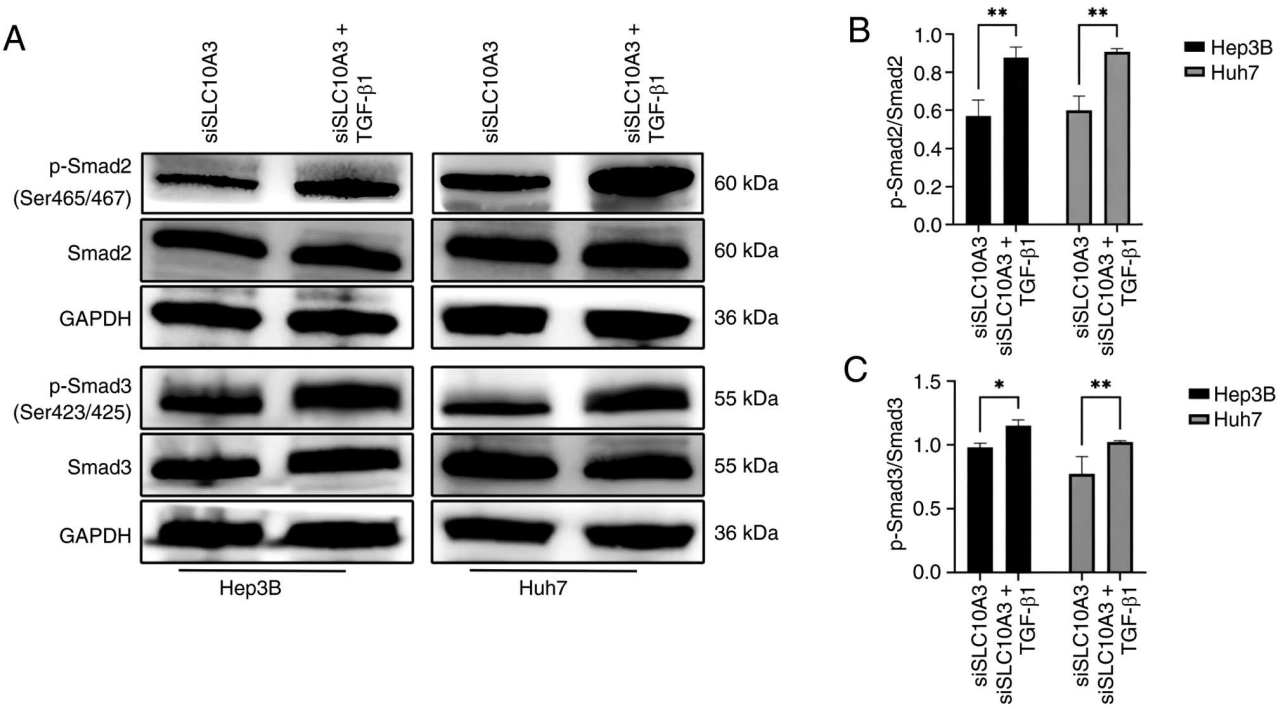


Figure 7. Impact of exogenous TGF-β1 on the TGF-β signaling pathway in liver cancer cells with SLC10A3 knockdown. (A) Western blot depicting alterations in the levels of core proteins of the TGF-β pathway following treatment with TGF-β1. (B) Semi-quantitative analysis was conducted to evaluate the (B) p-Smad2/Smad2 and (C) p-Smad3/Smad3 protein expression ratios based on the western blot bands shown in (A). *P<0.05, **P<0.01 vs. siSLC10A3. si, small interfering RNA; SLC10A3, solute carrier family 10 member 3; TGF-β, transforming growth factor-β.

signaling, thereby facilitating the malignant behaviors of LC cells.

The present study illustrated that SLC10A3 may contribute to the malignant phenotype of LC cells via modulation of TGF-β pathway signaling. However, several limitations still exist in the present study. First, the upstream mechanism by which SLC10A3 modulates the TGF-β/Smad signaling pathway was not investigated in the present study. Whether SLC10A3 directly interacts with the TGF-β receptor or regulates TGFBR1 activation remains unclear and requires further study. Second, the specific molecular mechanism associating SLC10A3 with altered TGF-β1 secretion has not been fully elucidated, and the detailed upstream regulatory events underlying this effect remain to be further clarified. Third, the present study lacks *in vivo* experimental validation, which hinders comprehensive understanding of the biological function of SLC10A3 and its crosstalk with the TME. This limitation should be addressed in future investigations. Fourth, the present study mainly focused on the effects of SLC10A3 on malignant phenotypes such as the proliferation, migration and invasion of LC cells, but did not further explore the specific role of the TGF-β signaling pathway (whose activity is altered by SLC10A3) in tumor immune regulation, nor did it verify the effects of SLC10A3 on immune responses during LC immunotherapy. This also represents a limitation of the present study, and relevant *in vivo* and *in vitro* validation remains to be performed in future research. Fifth, SLC10A3 overexpression rescue experiments were not performed in the present work. Therefore, the bidirectional role of SLC10A3 could not be further validated, and this issue remains to be investigated in future work. Sixth, beyond TGF-β signaling, SLC10A3 may affect LC progression through other uncharacterized pathways, which deserves further exploration.

Notably, LC exhibits prominent molecular and etiological heterogeneity, and hepatitis B (HBV)-, hepatitis C (HCV)- and non-alcoholic steatohepatitis (NASH)-related LC each display distinct driver gene profiles and basal TGF-β pathway activities (42,43). While this subtype-dependent difference has not been directly validated in the present study, based on the cited literature it was inferred that HBV-associated LC may represent a subtype with relatively higher reliance on the SLC10A3-TGF-β regulatory axis.

Recent studies have demonstrated that the HBV-encoded HBx protein is a potent upstream trigger for persistent TGF-β pathway hyperactivation, which continuously promotes TGF-β1 secretion and enhances TGF-βRI phosphorylation in hepatocarcinogenesis (44,45). Such constitutive TGF-β hyperactivation makes HBV-infected LC cells dependent on upstream modulators to sustain oncogenic TGF-β/Smad signaling (46). By contrast, HCV-related LC often acquires catenin β1 oncogenic mutations that can bypass partial TGF-β signaling requirements, which may weaken the dependence on the SLC10A3-TGF-β axis (47,48). NASH/metabolic dysfunction-associated steatohepatitis-associated LC is driven primarily by metabolic disorders and redox imbalance, with complex pathway crosstalk that diversifies malignant signaling and reduces exclusive reliance on the TGF-β cascade (49,50).

Therefore, the association between SLC10A3 and altered TGF-β signaling may exhibit prominent subtype specificity. It is speculated that SLC10A3-targeted strategies may offer

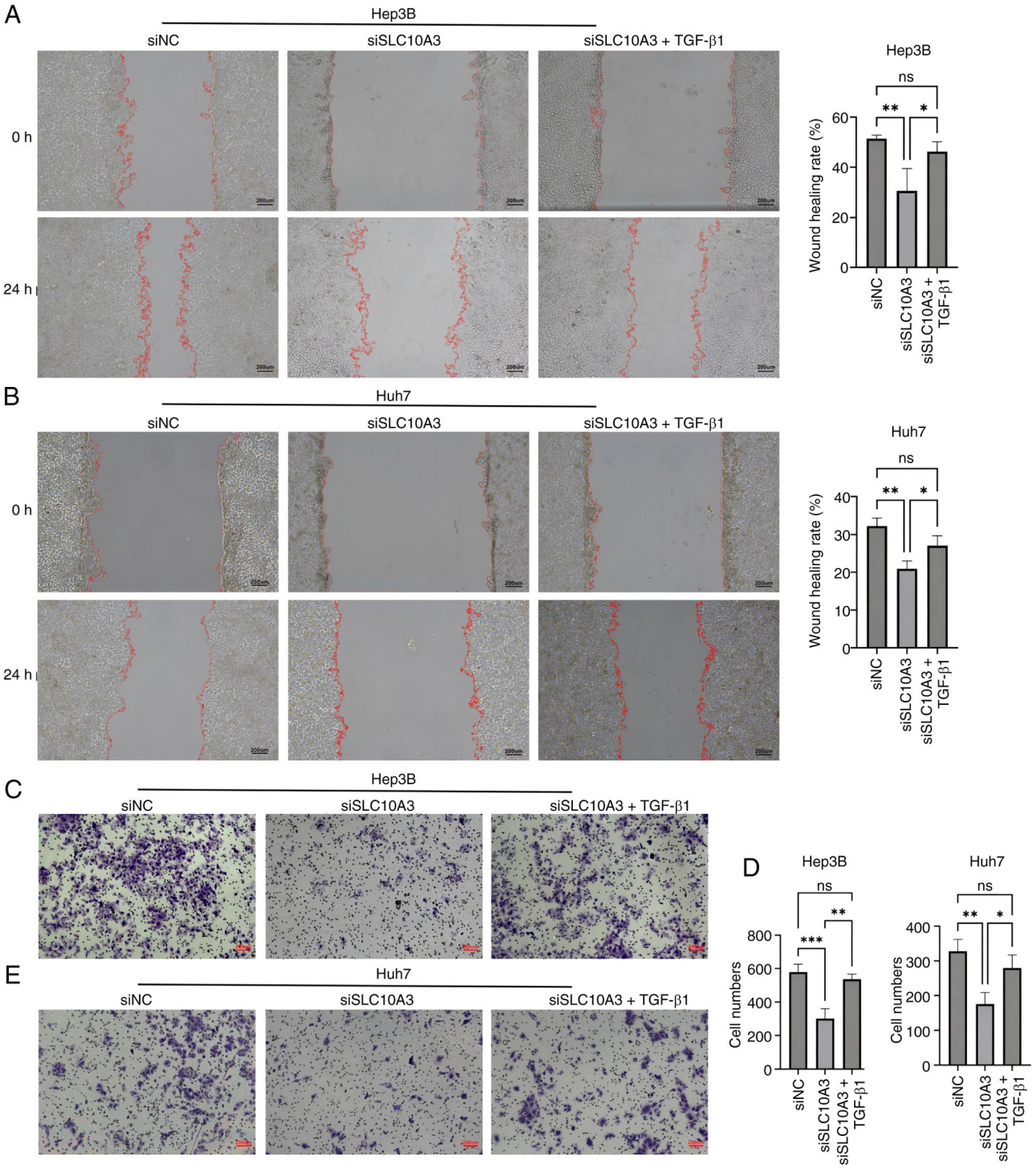


Figure 8. Impact of SLC10A3 downregulation and TGF-β1 exposure on liver cancer cell migration and invasion. (A) Wound healing assay for evaluating the migration rate of Hep3B cells. (B) Wound healing assay for evaluating the migration rate of Huh7 cells. (C) Transwell invasion assay for assessing the invasive capacity of Hep3B cells. (D) Quantitative analysis of the invasive ability of Hep3B and Huh7 cells across different groups. (E) Transwell invasion assay for assessing the invasive capacity of Huh7 cells. Scale bar, 200 μm; magnification, x100. *P<0.05, **P<0.01, ***P<0.001. si, small interfering RNA; NC, negative control; SLC10A3, solute carrier family 10 member 3; TGF-β, transforming growth factor-β.

a more precise therapeutic direction for HBV-positive LC, which remains to be confirmed by further subtype-specific studies.

In summary, the results of the present study suggest that SLC10A3 may serve as a predictive marker and therapeutic target in LC. Co-targeting SLC10A3 and the TGF-β pathway may represent a promising therapeutic strategy, especially for patients with LC harboring high SLC10A3 expression and hyperactivated TGF-β signaling, which may improve personalized treatment efficacy.

Acknowledgements

Not applicable.

Funding

The National Natural Science Foundation of China funded the present investigation (grant no. 82060541).

Availability of data and materials

The data generated in the present study may be found in the National Center for Biotechnology Information database under accession number PRJNA1426142 or at the following URL: https://www.ncbi.nlm.nih.gov/sra/PRJNA1426142.

Authors' contributions

OL, CY and MY were responsible for methodology/investigation. CY and MY were responsible for data curation and formal analysis. PP conceived and designed the study and interpreted the experimental results. OL was responsible for writing the original draft. OL and PP were responsible for reviewing and editing. CY and OL confirm the authenticity of all the raw data. All authors read and approved the final version of the manuscript.

Ethics approval and consent to participate

Not applicable.

Patient consent for publication

Not applicable.

Competing interests

The authors declare that they have no competing interests.

References

1. Sung H, Filho AM, Laversanne M, Ferlay J, Siegel RL, Soerjomataram I, Jemal A and Bray F: Global cancer statistics 2024: GLOBOCAN estimates of incidence and mortality worldwide for 34 cancers in 186 countries. CA Cancer J Clin 76: e70090, 2026.
2. Xin X, Cheng X, Zeng F, Xu Q and Hou L: The role of TGF-β/SMAD signaling in hepatocellular carcinoma: From mechanism to therapy and prognosis. Int J Biol Sci 20: 1436-1451, 2024.
3. Sung H, Ferlay J, Siegel RL, Laversanne M, Soerjomataram I, Jemal A and Bray F: Global cancer statistics 2020: GLOBOCAN estimates of incidence and mortality worldwide for 36 cancers in 185 countries. CA Cancer J Clin 71: 209-249, 2021.
4. Pham L, Kyritsi K, Zhou T, Ceci L, Baiocchi L, Kennedy L, Chakraborty S, Glaser S, Francis H, Alpini G and Sato K: The functional roles of immune cells in primary liver cancer. Am J Pathol 192: 826-836, 2022.
5. Petrowsky H, Fritsch R, Guckenberger M, De Oliveira ML, Dutkowski P and Clavien PA: Modern therapeutic approaches for the treatment of malignant liver tumours. Nat Rev Gastroenterol Hepatol 17: 755-772, 2020.
6. He Y, Song J, Qin Y, Mao D, Ding D, Wu S and Wu H: The prognostic significance and immune correlation of SLC10A3 in low-grade gliomas revealed by bioinformatic analysis and multiple immunohistochemistry. Aging (Albany NY) 15: 3771-3790, 2023.
7. Wang B, Fan W, Tao Y, Zhang S, Wang J, Fan Z, Liu L and Wang Y: The impact of SLC10A3 on prognosis and immune microenvironment in colorectal adenocarcinoma. Eur J Med Res 29: 20, 2024.
8. Tian S, Li J, Xiang J and Peng P: The clinical relevance and immune correlation of SLC10 family genes in liver cancer. J Hepatocell Carcinoma 9: 1415-1431, 2022.
9. Principe DR, Doll JA, Bauer J, Jung B, Munshi HG, Bartholin L, Pasche B, Lee C and Grippo PJ: TGF-β: Duality of function between tumor prevention and carcinogenesis. J Natl Cancer Inst 106: djt369, 2014.
10. Li H, Long D, Lv G, Cheng X, Wang G and Yang X: The double-edged sword role of TGF-β signaling pathway between intrauterine inflammation and cranial neural crest development. FASEB J 36: e22113, 2022.
11. Wrana JL, Attisano L, Wieser R, Ventura F and Massagué J: Mechanism of activation of the TGF-beta receptor. Nature 370: 341-347, 1994.
12. Derynck R and Zhang YE: Smad-dependent and Smad-independent pathways in TGF-beta family signalling. Nature 425: 577-584, 2003.
13. Lee JH and Massagué J: TGF-β in developmental and fibrogenic EMTs. Semin Cancer Biol 86 (Pt 2): 136-145, 2022.
14. Batlle E and Massagué J: Transforming growth factor-β signaling in immunity and cancer. Immunity 50: 924-940, 2019.
15. Livak KJ and Schmittgen TD: Analysis of relative gene expression data using real-time quantitative PCR and the 2(-Delta Delta C(T)) Method. Methods 25: 402-408, 2001.
16. Poursani EM, Mercatelli D, Raninga P, Bell JL, Saletta F, Kohane FV, Neumann DP, Zheng Y, Rouaen JRC, Jue TR, *et al*: Copper chelation suppresses epithelial-mesenchymal transition by inhibition of canonical and non-canonical TGF-β signaling pathways in cancer. Cell Biosci 13: 132, 2023.
17. Aiello NM and Kang Y: Context-dependent EMT programs in cancer metastasis. J Exp Med 216: 1016-1026, 2019.
18. Piccinno E, Scalavino V, Labarile N, Armentano R, Giannelli G and Serino G: miR-195-5p inhibits colon cancer progression via KRT23 regulation. Pharmaceutics 16: 1554, 2024.
19. Juaid N, Amin A, Abdalla A, Reese K, Alamri Z, Moulay M, Abdu S and Miled N: Anti-Hepatocellular carcinoma biomolecules: Molecular targets insights. Int J Mol Sci 22: 10774, 2021.
20. Li YZ, Deng J, Zhang XD, Li DY, Su LX, Li S, Pan JM, Lu L, Ya JQ, Yang N, *et al*: Naringenin enhances the efficacy of ferroptosis inducers by attenuating aerobic glycolysis by activating the AMPK-PGC1α signalling axis in liver cancer. Heliyon 10: e32288, 2024.
21. Zheng S, Su Z, He Y, You L, Zhang G, Chen J, Lu L and Liu Z: Novel prognostic signature for hepatocellular carcinoma using a comprehensive machine learning framework to predict prognosis and guide treatment. Front Immunol 15: 1454977, 2024.
22. Claro da Silva T, Polli JE and Swaan PW: The solute carrier family 10 (SLC10): Beyond bile acid transport. Mol Aspects Med 34: 252-269, 2013.
23. Sun Q, Lu H, Yuan F, Zhao Q, Wei Y, Wang R, Chen Q and Liu B: SLC10A3 regulates ferroptosis of glioblastoma through the STAT3/GPX4 pathway. Sci Rep 15: 21259, 2025.
24. Bintee B, Banerjee R, Hegde M, Manteghi N, Bhuyan P, Longkumar I, Ahmed GN, Baruah MN, Ahn KS and Kunnumakkara AB: Comprehensive big data analysis reveals SLC10A3 as a potential biomarker in head and neck cancer. Naunyn Schmiedebergs Arch Pharmacol 399: 6051-6081, 2026.
25. Ríos-López DG, Tecalco-Cruz AC, Martínez-Pastor D, Sosa-Garrocho M, Tapia-Urzúa G, Aranda-López Y, Ortega-Domínguez B, Recillas-Targa F, Vázquez-Victorio G and Macías-Silva M: TGF-β/SMAD canonical pathway induces the expression of transcriptional cofactor TAZ in liver cancer cells. Heliyon 9: e21519, 2023.
26. Wang J, Yu H, Dong W, Zhang C, Hu M, Ma W, Jiang X, Li H, Yang P and Xiang D: N6-Methyladenosine-mediated up-regulation of FZD10 regulates liver cancer stem cells' properties and lenvatinib resistance through WNT/β-catenin and hippo signaling pathways. Gastroenterology 164: 990-1005, 2023.
27. Xu C, Xu Z, Zhang Y, Evert M, Calvisi DF and Chen X: β-Catenin signaling in hepatocellular carcinoma. J Clin Invest 132: e154515, 2022.
28. Tian LY, Smit DJ and Jücker M: The role of PI3K/AKT/mTOR signaling in hepatocellular carcinoma metabolism. Int J Mol Sci 24: 2652, 2023.
29. Ho M, Thompson B, Fisk JN, Nebert DW, Bruford EA, Vasiliou V and Bunick CG: Update of the keratin gene family: evolution, tissue-specific expression patterns, and relevance to clinical disorders. Hum Genomics 16: 1, 2022.

30. Zhu Y, Huang C, Zhang C, Zhou Y, Zhao E, Zhang Y, Pan X, Huang H, Liao W and Wang X: LncRNA MIR200CHG inhibits EMT in gastric cancer by stabilizing miR-200c from target-directed miRNA degradation. Nat Commun 14: 8141, 2023.
31. Liu Y, Zhao Y, Song H, Li Y, Liu Z, Ye Z, Zhao J, Wu Y, Tang J and Yao M: Metabolic reprogramming in tumor immune microenvironment: Impact on immune cell function and therapeutic implications. Cancer Lett 597: 217076, 2024.
32. Liu S, Zhang X, Wang W, Li X, Sun X, Zhao Y, Wang Q, Li Y, Hu F and Ren H: Metabolic reprogramming and therapeutic resistance in primary and metastatic breast cancer. Mol Cancer 23: 261, 2024.
33. Wang J, Gong R, Zhao C, Lei K, Sun X and Ren H: Human FOXP3 and tumour microenvironment. Immunology 168: 248-255, 2023.
34. Wan M, Ding Y, Li Z, Wang X and Xu M: Metabolic manipulation of the tumour immune microenvironment. Immunology 165: 290-300, 2022.
35. Deng Z, Fan T, Xiao C, Tian H, Zheng Y, Li C and He J: TGF-β signaling in health, disease, and therapeutics. Signal Transduct Target Ther 9: 61, 2024.
36. Zaidi S, Gough NR and Mishra L: Mechanisms and clinical significance of TGF-β in hepatocellular cancer progression. Adv Cancer Res 156: 227-248, 2022.
37. Baba AB, Rah B, Bhat GR, Mushtaq I, Parveen S, Hassan R, Hameed Zargar M and Afroze D: Transforming growth factor-beta (TGF-β) signaling in cancer-A betrayal within. Front Pharmacol 13: 791272, 2022.
38. Guo J, Ma X, Liu D, Wang F, Xia J, Zhang B, Zhao P, Zhong F, Chen L, Long Q, *et al*: A distinct subset of urothelial cells with enhanced EMT features promotes chemotherapy resistance and cancer recurrence by increasing COL4A1-ITGB1 mediated angiogenesis. Drug Resist Updat 76: 101116, 2024.
39. Wang J, Xu Z, Wang Z, Du G and Lun L: TGF-beta signaling in cancer radiotherapy. Cytokine 148: 155709, 2021.
40. Ramundo V, Palazzo ML and Aldieri E: TGF-β as predictive marker and pharmacological target in lung cancer approach. Cancers (Basel) 15: 2295, 2023.
41. Jiang D, Qi Z, Xu Z and Li Y: CYB5D2 inhibits the malignant progression of hepatocellular carcinoma by inhibiting TGF-β expression and epithelial-mesenchymal transition. Oncol Res 33: 709-722, 2025.
42. Xing X, Hu E, Ouyang J, Zhong X, Wang F, Liu K, Cai L, Zhou Y, Wang Y, Chen G, *et al*: Integrated omics landscape of hepatocellular carcinoma suggests proteomic subtypes for precision therapy. Cell Rep Med 4: 101315, 2023.
43. Fujita M, Chen MM, Siwak DR, Sasagawa S, Oosawa-Tatsuguchi A, Arihiro K, Ono A, Miura R, Maejima K, Aikata H, *et al*: Proteo-genomic characterization of virus-associated liver cancers reveals potential subtypes and therapeutic targets. Nat Commun 13: 6481, 2022.
44. Yan W, Rao D, Fan F, Liang H, Zhang Z and Dong H: Hepatitis B virus X protein and TGF-β: Partners in the carcinogenic journey of hepatocellular carcinoma. Front Oncol 14: 1407434, 2024.
45. Guan Y, Li J, Sun B, Xu K, Zhang Y, Ben H, Feng Y, Liu M, Wang S and Gao Y, *et al*: HBx-induced upregulation of MAP1S drives hepatocellular carcinoma proliferation and migration via MAP1S/Smad/TGF-β1 loop. Int J Biol Macromol 28 1(Pt 3): 136327, 2024.
46. Liu Y, Xu Y, Ma H, Wang B, Xu L, Zhang H, Song X, Gao L, Liang X and Ma C: Hepatitis B virus X protein amplifies TGF-β promotion on HCC motility through down-regulating PPM1a. Oncotarget 7: 33125-33135, 2016.
47. Lu G, Lin J, Song G and Chen M: Prognostic significance of CTNNB1 mutation in hepatocellular carcinoma: A systematic review and meta-analysis. Aging (Albany NY) 15: 9759-9778, 2023.
48. Pezzuto F, Buonaguro L, Buonaguro FM and Tornesello ML: Frequency and geographic distribution of TERT promoter mutations in primary hepatocellular carcinoma. Infect Agent Cancer 12: 27, 2017.
49. Ghazanfar H, Javed N, Qasim A, Zacharia GS, Ghazanfar A, Jyala A, Shehi E and Patel H: Metabolic dysfunction-associated steatohepatitis and progression to hepatocellular carcinoma: A literature review. Cancers (Basel) 16: 1214, 2024.
50. Zhao J, Zhang Y, Wei Z, Li K, Sun L, Li D and Wang Y: The PI3K/Akt/mTOR Pathway: Immuno-Metabolic orchestration in IR/MASH-Associated hepatocellular carcinoma. Int J Biol Sci 21: 6025-6041, 2025.

Copyright © 2026 Long et al. This work is licensed under a Creative Commons Attribution-NonCommercial-NoDerivatives 4.0 International (CC BY-NC-ND 4.0) License.